The Impact of North Tropical Atlantic SST Anomalies in the Ensuing Spring of El Niño on the Tropical Indian Ocean and Northwest Pacific

Article *in* International Journal of Climatology · January 2020

DOI: 10.1002/joc.6500

5 authors, including:

Jing Ma
Nanjing University of Information Science & Technology
27 PUBLICATIONS **156** CITATIONS

Received: 24 July 2019 | Revised: 22 January 2020 | Accepted: 24 January 2020

DOI: 10.1002/joc.6500

RESEARCH ARTICLE

International Journal of Climatology RMetS

The impact of north tropical Atlantic sea surface temperature anomalies in the ensuing spring of El Niño on the tropical Indian Ocean and Northwest Pacific

Jing Ma | **Weibang He** | **Zhehan Chen** | **Yihang Fu** | **Jiayue Yin**

Collaborative Innovation Center on Forecast and Evaluation of Meteorological Disasters/KLME/ILCEC, Nanjing University of Information Science and Technology, Nanjing, China

Correspondence
Jing Ma, Collaborative Innovation Center on Forecast and Evaluation of Meteorological Disasters/KLME/ILCEC, Nanjing University of Information Science and Technology, No. 219 Ningliu Road, Pukou District, Nanjing, Jiangsu Province, 210044, China.
Email: majing@nuist.edu.cn

Funding information
National Key Research and Development Program of China, Grant/Award Number: 2017YFA0604100; National Natural Science Foundation of China, Grant/Award Number: 41805051; Startup Foundation for Introducing Talent of NUIST, Grant/Award Number: 2017r057

Abstract

Based on the fifth generation reanalysis of European Centre for Medium–Range Weather Forecasts (ECMWF), Hadley Centre sea ice and sea surface temperature data, and ENSEMLES hindcasts, the impact of north tropical Atlantic (NTA) sea surface temperature (SST) anomalies in the ensuing spring of El Niño on the tropical Indian Ocean (TIO) and Northwest Pacific (NWP) is investigated using composites, singular value decomposition, and correlations. The anomalous SST warming in the NTA region in the decay spring of El Niño leads to a Gill-type response of the overlying atmosphere in spring–summer. The Kelvin wave over the TIO stimulated by the NTA warming causes the anomalous easterlies in the regions of TIO and NWP, thereby the strengthening of the NWP subtropical anticyclone (NWPSA). The NTA SST warming also forces a local ascending motion, leading to a downward branch over the NWP region. This descent gives rise to the TIO-NWP low-level easterly anomalies and an intensification of the NWPSA. The anomalous easterly weakens the background southwesterly monsoon, accompanied by the increased atmospheric boundary layer specific humidity caused by the troposphere warming, suppressing upward latent heat fluxes, finally contributing to the North Indian Ocean (NIO) warming in summer. This indicates that the second warming of the NIO region in the following summer of El Niño may be partially attributed to the NTA warming in the ensuing spring of El Niño. This study improves our understanding of the impact of the NTA SST anomalies in the El Niño decay spring on the TIO and NWP regions, and emphasizes the importance of the NTA region in the pantropical inter-basin interactions.

KEYWORDS

El Niño, north tropical Atlantic Ocean, Northwest Pacific, tropical Indian Ocean, Gill-type response

1 | INTRODUCTION

El Niño-Southern Oscillation (ENSO) shows the most prominent interannual variability in the tropical Pacific, which exerts significant impacts on the global climate via atmospheric teleconnection by altering the sources of atmospheric heating (Trenberth *et al*., 1998; Klein *et al*., 1999; Wang *et al*., 2000; Alexander and Scott, 2002; Deser

et al., 2010; Xie *et al*., 2016; Jiang *et al*., 2018). El Niño is strongly phase-locked onto the annual cycle, typically peaking during winter and decaying in the following spring.

El Niño teleconnection induces a significant basin-wide warming over the tropical Indian Ocean on interannual timescale (TIO; Klein *et al*., 1999). Particularly, the north Indian Ocean (NIO) displays a peculiar double-peak warming, and the second peak is larger in magnitude and persists through the summer when El Niño itself has dissipated. Internal ocean–atmosphere interaction in the TIO plays a fundamental role in sustaining the TIO warming through summer (Du *et al*., 2009). The TIO warming, acting as a discharging capacitor, giving rise to atmospheric anomalies in the following summer of El Niño, including suppressed convection and an intensified Northwest Pacific (NWP) subtropical anticyclone (NWPSA) associated with an eastward propagating warm Kelvin wave triggered by the TIO warming (Yang *et al*., 2007; Xie *et al*., 2009, 2010, 2016; Li *et al*., 2017; Chowdary *et al*., 2019; Zhou *et al*., 2019). In addition, some studies showed that El Niño events with different decaying phases have different impacts on the NWPSA and Indian summer monsoon rainfall (Chen *et al*., 2012, 2016; Chowdary *et al*., 2017).

ENSO can also exert an impact on the north tropical Atlantic (NTA) sea surface temperature (SST) in spring (March–April–May, MAM) on interannual timescale mainly due to the following four mechanisms. The first proposes that the tropical Pacific forced Rossby wave train (Pacific-North American pattern), characteristic of a quadripole pattern of 500-hPa height anomalies, crosses the North Pacific-American sector, finally contributing to the NTA SST anomalies (Enfield and Mayer, 1997; Giannini *et al*., 2000, 2001). The second mechanism put forward a more direct atmospheric bridge, leading to modifications of the Atlantic Hadley circulation resulting from perturbations over the equatorial Atlantic convective region in response to changes of the Pacific Walker circulation (Klein *et al*., 1999; Wang, 2004). The third is the tropospheric temperature mechanism (Chiang and Sobel, 2002; Chiang and Lintner, 2005; Chang *et al*., 2006), in which upper-tropospheric temperature anomalies are related to the surface via moist convection processes. The anomalous temperature signal in the upper troposphere implies the eastward propagation of a Kelvin wave front triggered from the ENSO heating anomaly in the tropical Pacific (Lin *et al*., 2007; Lintner and Chiang, 2007). García–Serrano *et al*. (2017) identified the fourth mechanism that relies on the remote Gill-type response to the ENSO zonally compensated heat source over the Amazon basin, with anomalous diabatic cooling for El Niño events.

Some studies investigated the impact of the Atlantic SST anomalies on the Indian Ocean (IO) and NWP regions on interannual timescale (Rong *et al*., 2010; Ham *et al*., 2013; Hong *et al*., 2014, 2015; Chen *et al*., 2014a, 2014b, 2015; Jin and Huo, 2018). Hong *et al*. (2014, 2015), Jin and Huo (2018) found that the tropical Atlantic (TA) SST warming can cause modifications of the zonally overturning circulation, and the anomalous descent over the central Pacific acts to enhance the NWPSA. In addition, some studies identified the role of an eastward propagating teleconnection from the TA to the IO and adjacent regions, in which Kelvin waves act to transport the SST signal in the TA region (Kucharski *et al*., 2007, 2008, 2009; Li *et al*., 2016; Kamae *et al*., 2017).

Lee *et al*. (2008) showed that the duration of the El Niño events is crucial for its spring teleconnection to the NTA region, and only the El Niño events that persist into spring can force a significant SST warming over the NTA region. Therefore, the following questions need to be addressed. Can NTA SST anomalies in the ensuing spring of El Niño impact the TIO and NWP regions? Does the NTA SST anomaly play a role in the second warming of the NIO region? If so, what is the underlying mechanism?

The remainder of this paper is organized as follows. Section 2 introduces the data and methods. Section 3 shows the observational results. Section 4 investigates the impact of the NTA warming in the ensuing spring of El Niño on the TIO and NWP regions based on the hindcasts. Section 5 provides the summary and discussion.

2 | DATA AND METHODS

Monthly SST data from Hadley Centre sea ice and sea surface temperature (HadISST; Rayner *et al*., 2003) are used for the period 1960–2005. It has a horizontal resolution of $1^\circ \times 1^\circ$. We also use the monthly atmospheric variables for the period of 1980–2005 from the fifth generation reanalysis of European Centre for Medium-Range Weather Forecasts (ECMWF) with a horizontal resolution of $0.25^\circ \times 0.25^\circ$ and 37 pressure levels vertically, including winds, sea level pressure (SLP), SST, and precipitation [Copernicus Climate Change Service (C3S), 2017].

This study also uses the hindcasts of ENSEMBLES, which is a multi-model ensemble system developed by the European Union (van der Linden and Mitchell, 2009). The ENSEMBLES includes five fully coupled atmosphere–ocean–land models from the ECMWF, the Leibniz Institute of Marine Sciences at Kiel University (IFM-GEOMAR), the Météo-France (MF), the UK Met Office (UKMO), and the Euro-Mediterranean Center for

Climate Change (CMCC-INGV). The ENSEMBLES hindcasts successfully reproduce the interannual variability of ENSO and well capture the different ENSO phases (Li *et al*., 2014).

The hindcasts of all five models for the period of 1960–2005 are used in this study. Seasonal hindcasts with a length of 7 months starting on the first of February, May, August, and November were carried out for each year. Additionally, the November-initialized hindcasts from all the models except for CMCC-INGV were extended to 14-month-long annual forecasts. The individual model ensembles consist of nine members only differing in initial conditions. In this study, we use the hindcasts initialized from February to focus on the ensuing spring–summer of El Niño.

Singular value decomposition (SVD) can be used to find covariant patterns in two different variable fields. SVD operates on the covariance matrix and provides pairs of spatial modes with high temporal covariance. Further details on SVD analysis in meteorology can be found in Deser and Timlin (1997). Similar to Ma *et al*. (2017a, 2017b), an SVD analysis is performed on a concatenated 5 models by 9 members by 46 years record of the MAM averaged fields in the ENSEMBLES hindcasts. For example, the SST matrix is (Nx, Ny, Nens, Nyr), where Nx and Ny are the zonal and meridional grid numbers, respectively, Nens denotes the ensemble number, and Nyr represents the number of years. We focus on the inter-member variability by subtracting the ensemble mean (Nx, Ny, Nyr) from the matrix (Nx, Ny, Nens, Nyr). Then, the matrix (Nx × Ny, Nens × Nyr) is used for the SVD analysis. Hence, the conventional time dimension is enlarged by the ensemble size. Similarly, we obtain the inter-annual anomalies by calculating the deviations from the climatological mean.

To clearly show the relationship between winds, SLP, precipitation, etc. and the coupled modes, correlation and regression coefficients are calculated. The Student's *t* test is used to evaluate the significance of correlations.

3 | OBSERVATIONAL RESULTS

El Niño events are defined based on the above-normal Niño3.4 SST anomalies with a threshold of 0.5 K for six consecutive months. Thus, 11 El Niño events are identified using observations for the period of 1960–2005, including 1963/1964, 1965/1966, 1969/1970, 1972/1973, 1982/1983, 1987/1988, 1991/1992, 1994/1995, 1997/1998,

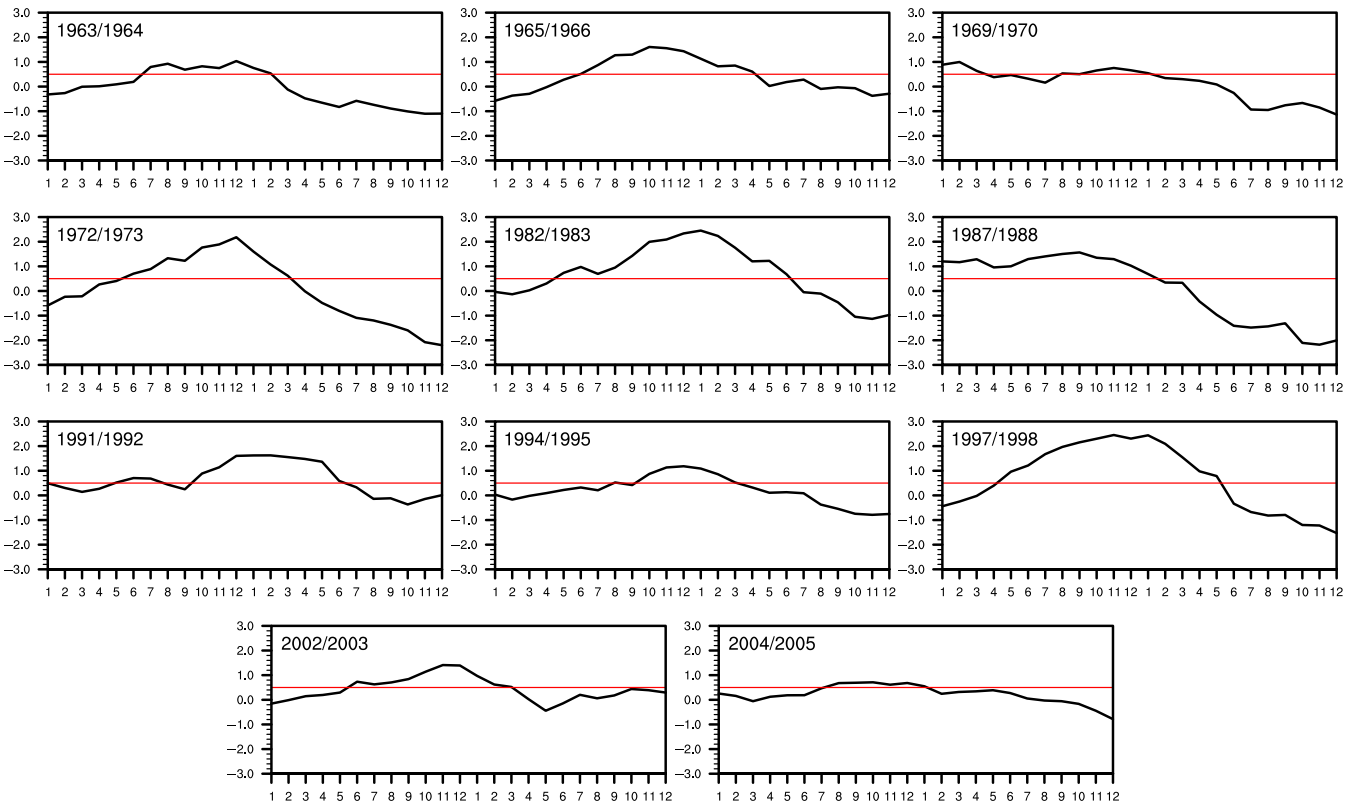

FIGURE 1 Niño3.4 SST anomalies (units: K) for all the 11 El Niño events from 1960 to 2005 in observations. The red lines show the threshold of 0.5 K [Colour figure can be viewed at wileyonlinelibrary.com]

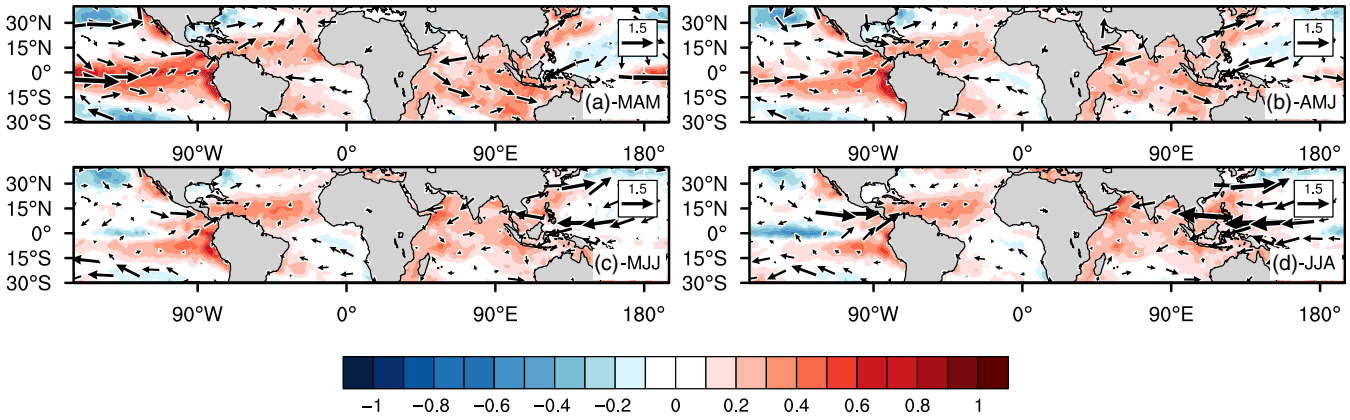

FIGURE 2 Composites of the SST (colour shadings; units: K) and 850-hPa wind (vectors; units: m s^{-1}) anomalies over the tropical Atlantic, TIO, and NWP regions in (a) MAM(1), (b) AMJ(1), (c) MJJ(1), and (d) JJA(1). "(1)" denotes the decay year of the El Niño event, the same hereafter [Colour figure can be viewed at wileyonlinelibrary.com]

2002/2003, and 2004/2005 (Figure 1). Accordingly, 11 El Niño decay years are obtained.

Figure 2 shows the composites of the SST and 850-hPa wind anomalies over the tropical Atlantic, TIO, and NWP regions in the ensuing spring–summer of the El Niño events. Anomalous SST warming prevails over the NTA region from spring to summer. Positive SST anomalies also occur in the southwestern Atlantic region. However, they shrink from spring to summer, only with a small patch in summer. In addition, the TIO region warms up in spring with strongest positive anomalies near the equator and southeastern Indian Ocean. Positive SST anomalies migrate northward from spring to summer. Thus, noticeable SST warming is located over the NIO region in summer, including the Arabian Sea, Bay of Bengal (BOB), and South China Sea (SCS).

The 850-hPa wind anomalies over the Atlantic region in spring are characteristic of southwesterly anomalies in the NTA region and easterly anomalies near the equator. The southwesterly anomalies in the NTA region decelerate the background northeasterly trade winds, finally inducing the SST warming via suppressing the latent heat fluxes. This is consistent with previous studies (Klein *et al*., 1999; Giannini *et al*., 2000, 2001), which show that latent heat flux variations associated with those in the trade wind intensity in spring contribute to the ENSO-related NTA SST anomaly, mediated by the wind-evaporation-SST (WES) feedback (Xie and Philander, 1994). The easterly anomalies near the equator contribute to the SST cooling in the following months (Figures 2b–d), mainly arising from the Bjerknes feedback (Bjerknes, 1969). Note that the wind anomalies over the Atlantic region weaken gradually from spring to summer.

Easterly anomalies occur over the NIO and NWP regions. The anomalous easterlies decelerate the background southwesterly monsoon wind, giving rise to the NIO SST warming, which in turn causes easterly anomalies by triggering a Kelvin wave response (Yang *et al*., 2007; Du *et al*., 2009; Xie *et al*., 2009, 2016). This constitutes a positive feedback loop. The easterly anomalies intensify from spring to summer, accompanied by a strengthened anticyclone located in the NWP region, indicative of an intensification of the NWPSA via Ekman divergence off the equator (Xie *et al*., 2009).

The SLP and precipitation anomalies in the following spring–summer of the El Niño events are shown in Figure 3. Precipitation over the NTA region is above normal from spring to summer, with the most significant surplus located near 10°N. Negative precipitation anomalies sit near the equator. The largest positive precipitation anomalies occur in MJJ (May–June–July). Over the TIO region, above-normal precipitation anomalies move northward from spring to summer, with the largest precipitation anomalies over the NIO region in summer. The northward migration of the precipitation is closely related to the northward movement of positive SST anomalies in the TIO region (Figure 2). The precipitation is below normal in the NWP region, linked to the strengthened NWPSA.

Consistent with the precipitation anomalies, negative SLP anomalies are located over the NTA region, which weaken gradually from spring to summer. In the NWP region, positive SLP anomalies strengthen from spring to summer, indicating the intensification of the NWPSA.

To investigate the impact of the NTA SST anomalies in the ensuing spring of El Niño on the TIO and NWP regions, we obtain the SST anomalies averaged in the NTA region (0–20°N, 70°W–15°E) by subtracting the climatological mean from the raw SST, referred to as the NTASST hereafter. We classify the years with the

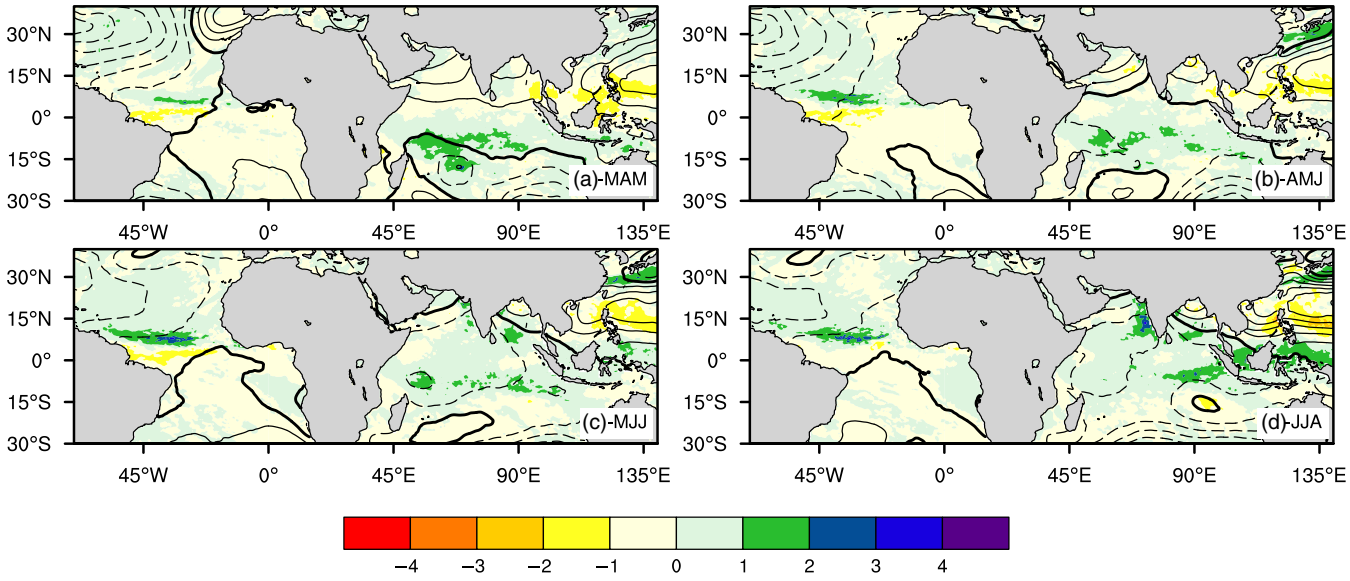

FIGURE 3 Composites of the precipitation (colour shadings; units: mm d^{-1}) and SLP (contours at an interval of 0.2; units: hPa) anomalies over the tropical Atlantic, TIO, and NWP regions in (a) MAM(1), (b) AMJ(1), (c) MJJ(1), and (d) JJA(1) [Colour figure can be viewed at wileyonlinelibrary.com]

NTASST larger than 0 as warm cases, including 1983, 1988, 1995, 1998, and 2005, while those with the NTA SST smaller than 0 as cold cases, containing 1992 and 2003.

Figure 4a–d shows the composites of the SST and 850-hPa wind anomalies over the tropical Atlantic, TIO, and NWP regions for the warm cases. The NTA warming is accompanied by the TIO warming from spring to

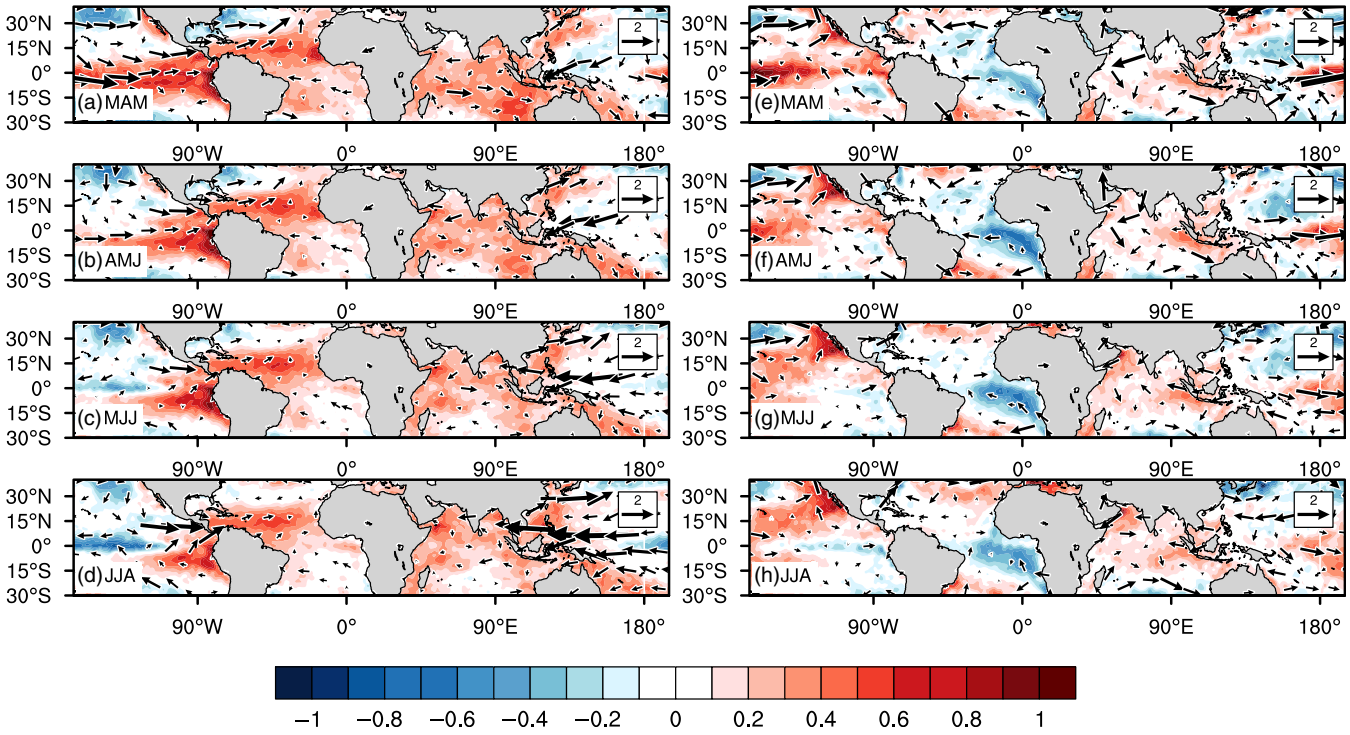

FIGURE 4 Composites of the SST (colour shadings; units: K) and 850-hPa wind (vectors; units: m s^{-1}) anomalies over the tropical Atlantic, TIO, and NWP regions in (a) MAM(1), (b) AMJ(1), (c) MJJ(1), and (d) JJA(1) for the warm cases. Panels 4e–h are the same as panels 4a–d, but for the cold cases [Colour figure can be viewed at wileyonlinelibrary.com]

summer. The positive TIO SST anomalies moves northward with months. The composites of the SST and 850-hPa wind anomalies for the cold cases (Figure 4e–h) show that the TIO warming persists even with an anomalous cold NTA ocean. However, the TIO warming weakens remarkably compared to the warm cases. This suggests that the NTA SST warming is favourable for the TIO warming, although it cannot change the positive sign of the SST anomalies which mainly arise from the preceding El Niño event. Additionally, this also indicates that the second warming of the NIO may be partially attributed to the impact of the NTA warming.

In the warm cases, southwesterly anomalies occur over the NTA region, contributing to the NTA warming via the WES feedback (Xie and Philander, 1994). Easterly anomalies prevail near the equator in the cold cases, causing SST cooling in the tropical Atlantic, especially in the southeastern Atlantic, which is typical of an Atlantic Niño, rooted in the Bjerknes feedback (Bjerknes, 1969). In the eastern TIO region including the BOB and SCS regions, wind anomalies exhibit a significant difference between the warm and cold cases, with and without large easterly anomalies, respectively. The easterly anomalies in the warm cases can cause surface divergence over the NWP region, which further triggers the local suppression of convection, giving rise to the strengthening of the NWPSA (Xie *et al*., 2009). This suggests that the NTA SST warming contributes to an intensification of the NWPSA, consistent with previous studies (Rong *et al*., 2010; Ham *et al*., 2013; Hong *et al*., 2014, 2015; Chen *et al*., 2014a, 2014b, 2015; Jin and Huo, 2018). Note that weak easterly anomalies correspond to the weak SST warming over the TIO region in the cold cases due to a weak WES feedback (Xie and Philander, 1994).

4 | HINDCAST RESULTS

4.1 | Composite analyses

4.1.1 | The first method of composite analyses

The observational result shows that the NTA SST anomalies in the ensuing spring of El Niño may impact the TIO and NWP regions. However, the El Niño cases are very limited in observations, rendering it difficult to confirm the role of the NTA SST anomalies. The ENSEMBLES hindcasts provide us more El Niño cases, enabling the examination of the impact of the NTA SST anomalies on the TIO and NWP regions and the underlying mechanism by reducing the signal-to-noise ratio.

First, we obtain the SST anomalies by subtracting the climatological mean SST (Nx, Ny, Nens) from the matrix (Nx, Ny, Nens, Nyr) in all the ensuing springs of the El Niño events. Then the SST anomalies averaged in the NTA region identify 366 warm cases and 44 cold cases. Warm cases are much more than cold ones, similar to observations. This is referred to as the first method of the composite analyses.

The composites of the SST and 850-hPa wind anomalies over the tropical Atlantic, TIO, and NWP regions for the warm cases are illustrated in Figure 5a–d. The SST and 850-hPa wind patterns generally agree with the observational results, with positive SST anomalies in both the NTA and TIO regions, southwesterly and easterly anomalies over the NTA and equatorial Atlantic regions, respectively, and an intensification of the NWPSA. SST anomalies in the equatorial TIO region are still positive in the cold cases (Figure 5e–h), but with a much smaller magnitude compared to the warm cases (Figure 5a–d). Correspondingly, the wind anomalies over the NWP region significantly weaken in the cold cases in comparison with the warm ones. This confirms that the NTA SST anomalies exert an important impact on the TIO and NWP regions, in support of the observational finding. The second warming of the NIO may partially arise from the impact of the NTA warming. In addition, of note is that the SST anomalies in the south Atlantic region are different from those in observations (Figure 4e–h), which may be related to the weak Bjerknes feedback (Bjerknes, 1969) in the hindcasts arising from that no significant zonal wind anomalies occur.

4.1.2 | The second method of composite analyses

To highlight the impact of the NTA SST anomalies, we focus on the inter-member variability by subtracting the ensemble mean (Nx, Ny, Nyr) from the matrix (Nx, Ny, Nens, Nyr) in all the ensuing springs of the El Niño events, where "Nyr" equals 11. Then we define an SST anomaly series by averaging the SST in the NTA region, based on which we identify 157 warm cases and 189 cold cases. This is the second method of the composite analyses.

Figure 6 presents the composites of the SST and 850-hPa wind anomalies over the tropical Atlantic, TIO, and NWP regions for the warm and cold cases. The NTA warming and concurrent warming of the TIO in the warm cases, and the simultaneous SST cooling in the cold cases stand out. This again demonstrates the important role of the NTA SST warming in the second SST warming of the NIO region. Different from Du *et al*.

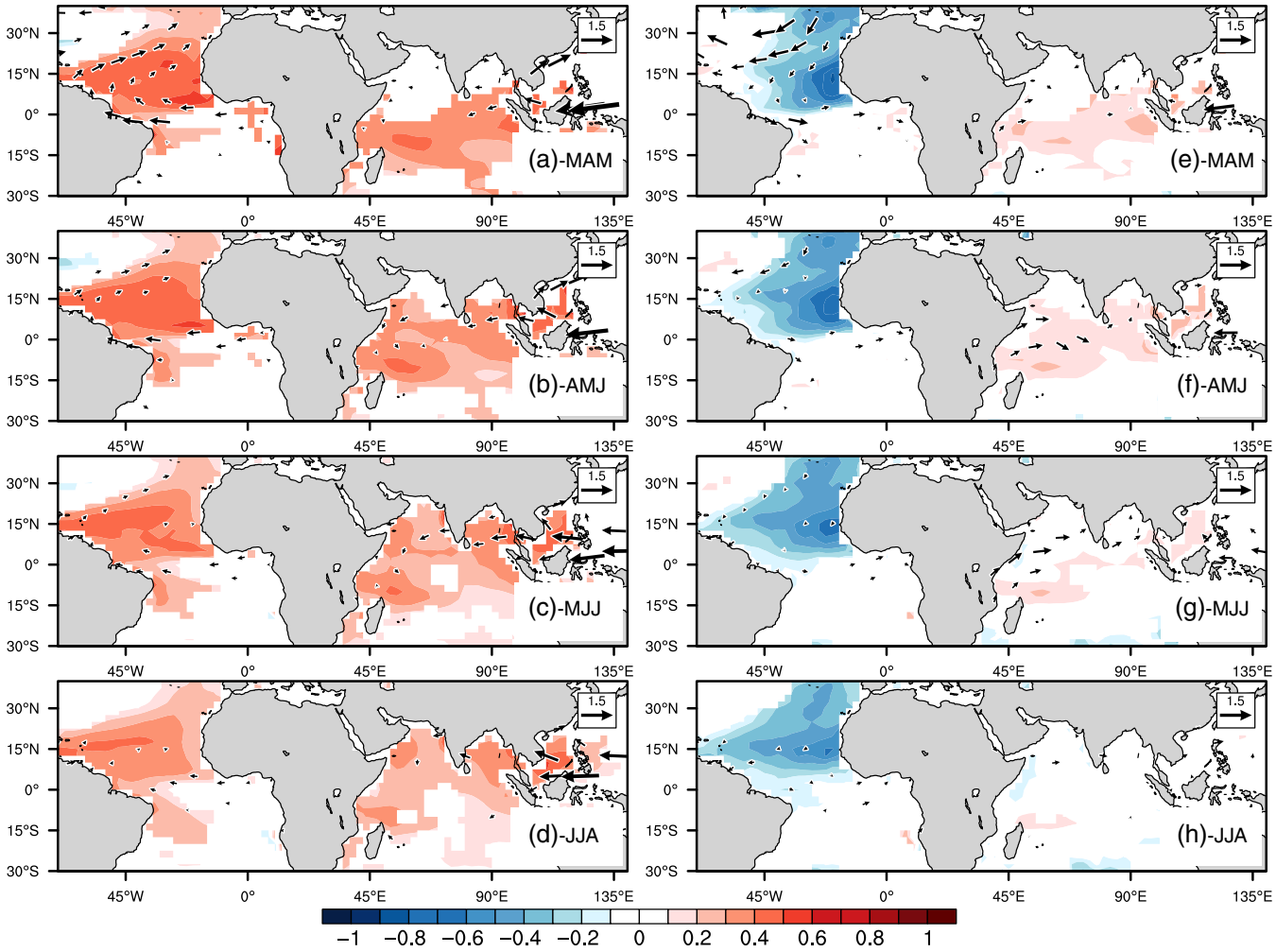

FIGURE 5 Composites of the SST (colour shadings; units: K) and 850-hPa wind (vectors; units: m s^{-1}) anomalies over the tropical Atlantic, TIO, and NWP regions in (a) MAM(1), (b) AMJ(1), (c) MJJ(1), and (d) JJA(1) for the warm cases obtained by subtracting the climatological mean from the raw SST in the hindcasts. Panels e–h are the same as panels a–d, but for the cold cases. Only the anomalies significant at the 95% confidence level are shown [Colour figure can be viewed at wileyonlinelibrary.com]

(2009) which emphasized the contribution of the local ocean–atmosphere interaction, this study reveals the impact of the NTA SST anomalies. The wind anomalies in the cold cases are generally opposite to those in the warm cases, implying the role of the WES feedback in the SST anomalies (Xie and Philander, 1994).

4.2 | SVD analyses

To further show the influence of the NTA SST anomalies in the ensuing spring of El Niño on the TIO and NWP regions, SVD analyses are conducted. First, we focus on the interannual variability of the SST by subtracting the climatological mean (Nx, Ny, Nens) from the matrix (Nx, Ny, Nens, Nyr) in all the ensuing springs of the El Niño events. Then, the matrix (Nx × Ny, Nens × Nyr) is used for the SVD analysis. We perform SVD analysis between the SST anomalies over the TIO-NWP region (left field, 20°S–20°N, 40°–100°E) and those over the NTA region (right field, 0–20°N, 110°W–15°E) in spring. The first SVD mode accounts for 95.91% the total covariance. The correlation coefficient between the first principal component (PC1) of the left and right heterogeneous fields reaches 0.66. This indicates that the first mode dominates the SST covariability between these two regions.

Besides, we also perform an SVD analysis for the inter-member variability of the SST by subtracting the ensemble mean (Nx, Ny, Nyr) from the matrix (Nx, Ny, Nens, Nyr) in all the ensuing springs of the El Niño events, where "Nyr" equals 11. Similarly, we perform SVD analysis between the SST anomalies over the TIO-NWP region and those over the NTA region in spring. The first SVD mode explains 96.21% the total covariance with the correlation coefficient between the PC1 of the left and right heterogeneous fields of 0.55. The first mode

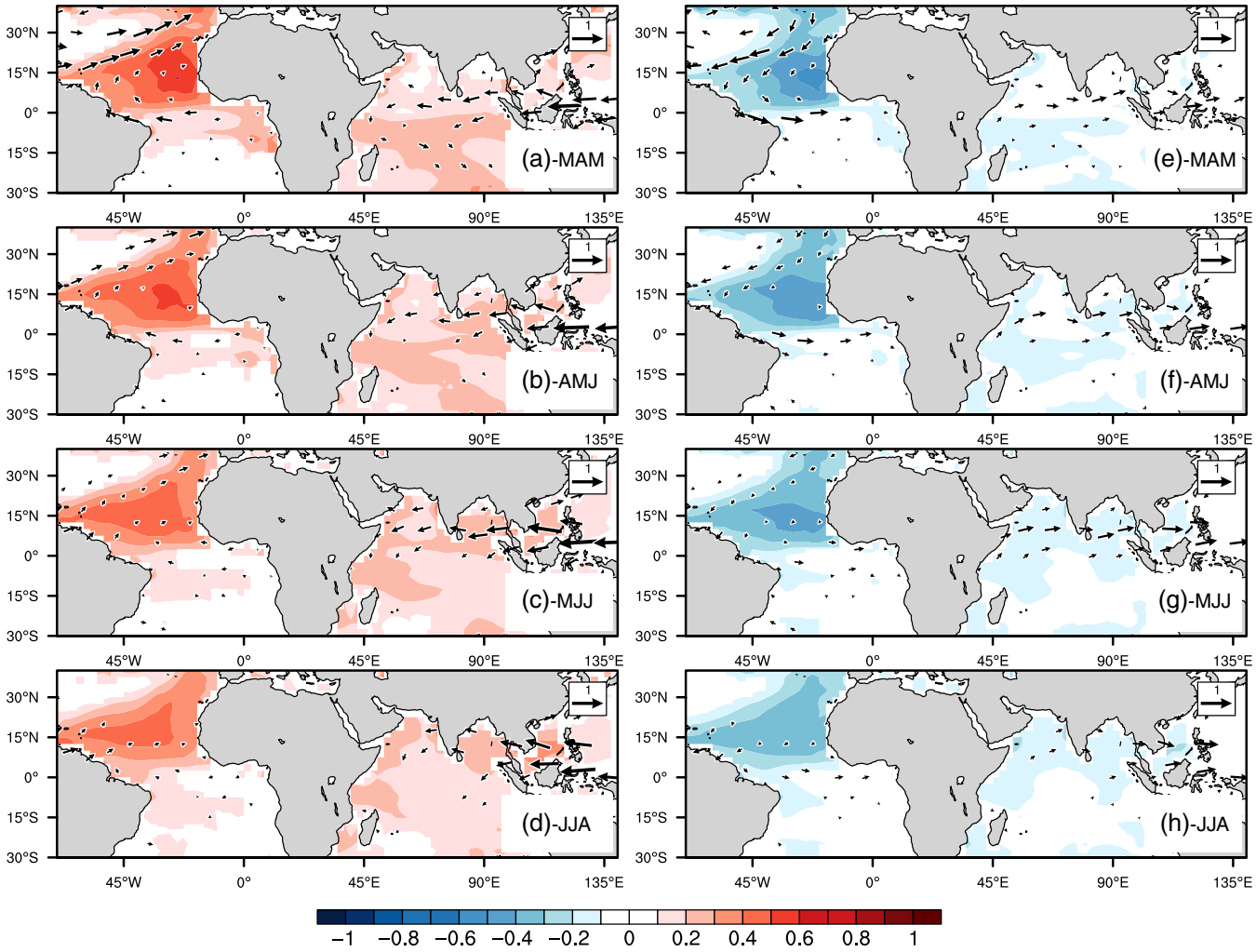

FIGURE 6 Same as Figure 5, but for the warm and cold cases obtained by subtracting the ensemble mean from the raw SST in the hindcasts [Colour figure can be viewed at wileyonlinelibrary.com]

almost fully represents the SST covariability between these two regions.

Figure 7a–d illustrates the correlation coefficients between the SST, 850-hPa wind anomalies and the PC1 of the right heterogeneous field (NTA SST anomalies) of the SVD analysis for the interannual anomalies of SST. They share consistency with the composite results in Figure 6a–d, confirming the important role of the NTA SST warming in the second SST warming of the NIO region. The correlation coefficients between the SST and 850-hPa wind anomalies and the PC1 of the right heterogeneous field of the SVD analysis for the inter-member SST anomalies (Figure 7e–h) are generally similar to Figure 7a–d, implying that the internal dynamics contribute significantly to the interannual variability of the SST. Note that the SST anomalies over the NTA region weaken from spring to summer, while those over the NIO region become stronger from spring to summer. This indicates that the SST variability over the NTA region gradually dissipates, while that over the NIO region strengthens with stronger easterly anomalies. This implies the lag effect of the NTA SST anomalies on the NIO and NWP regions. Both the two SVD results confirm the important role of the NTA SST anomalies during the ensuing spring of El Niño in the SST variability over the TIO and NWP regions in spring–summer, and the second warming of the NIO region in the following summer of El Niño may be partially attributed to the NTA warming in the preceding spring.

Due to the similarity between these two SVD results, the following study focuses on the SVD result based on the inter-member variability of the SST. Figure 8a–d shows the correlation coefficients between the SLP, precipitation anomalies and the PC1 of the right heterogeneous field of the SVD analysis for the inter-member anomalies of SST. In the ensuing spring of El Niño, in response to the SST warming over the NTA region, precipitation increases and decreases to the north and near

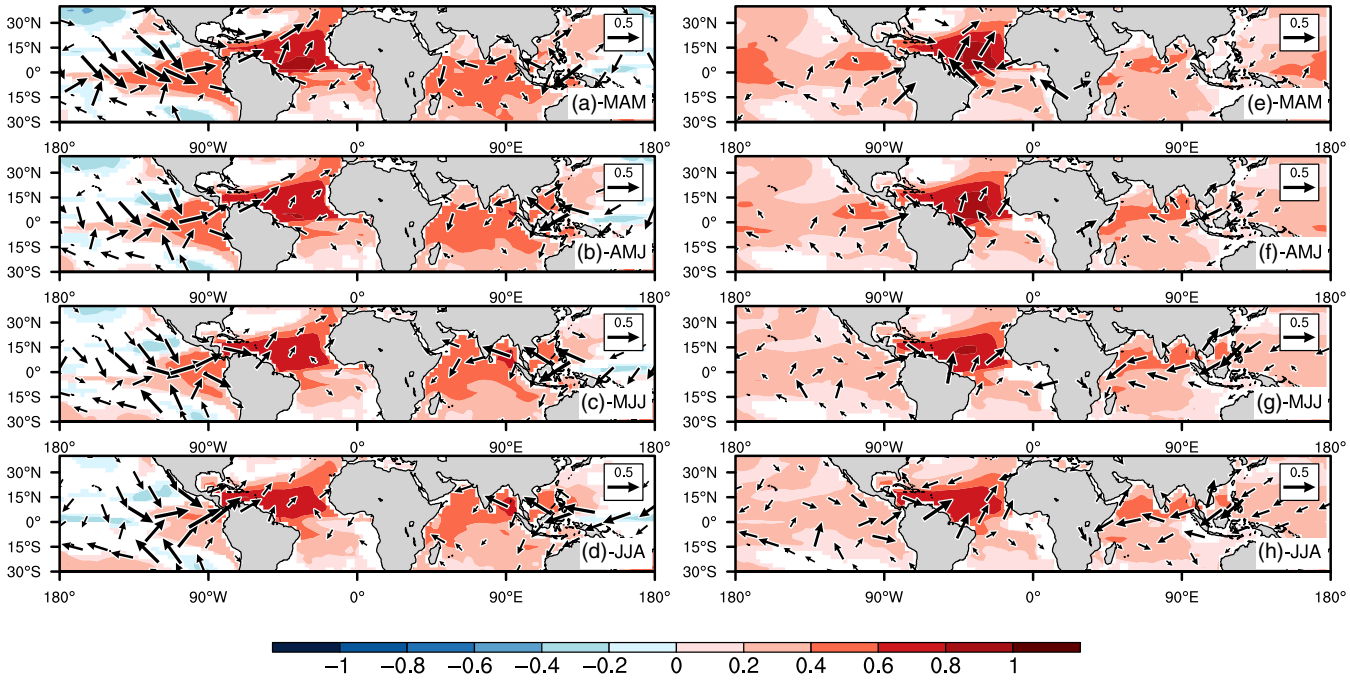

FIGURE 7 Correlation coefficients between the SST (colour shadings) and 850-hPa wind (vectors) anomalies in (a) MAM(1), (b) AMJ (1), (c) MJJ(1), and (d) JJA(1) and the PC1 of the right heterogeneous field of the SVD analysis for the interannual anomalies of SST over the tropical Atlantic, TIO, and NWP regions in the hindcasts. Panels e–h are the same as panels a–d, but for the SVD analysis for the inter-member anomalies of SST. Only the correlations significant at the 95% confidence level are shown. The Student's *t* test is used to evaluate the significance of correlations, and the same hereafter [Colour figure can be viewed at wileyonlinelibrary.com]

the equator, respectively, sharing some consistency with the observational precipitation pattern shown in Figure 3. This implies that the Intertropical Convergence Zone over Atlantic is shifted northward corresponding to the NTA SST warming. The positive precipitation anomalies march northwestward in response to the SST warming over the NTA region, associated with the northward migration of the climatological mean SST from spring to summer (not shown). The distribution of precipitation relates to the SLP decreases over the NTA region. In the western TIO region, SLP decreases accompanied by above-normal precipitation. Additionally, the positive precipitation anomalies enhance from spring to summer. SLP increases over the NWP region, collocated with the below-normal precipitation. This is associated with the strengthening of the NWPSA, as shown in Figures 6a–c and 7.

To understand the mechanism for the influence of the NTA SST anomalies on the TIO and NWP regions, we calculate the correlation coefficients between the tropospheric mean temperature, 500-hPa geopotential height, wind anomalies and the PC1 of the right heterogeneous field of the SVD analysis for the inter-member anomalies of SST (Figure 8e–h). In the ensuing spring–summer of El Niño, the NTA SST warming causes the tropospheric mean temperature and 500-hPa geopotential height over the tropical Atlantic, TIO, and NWP regions to increase. Tropospheric mean temperature anomalies exhibit a Gill pattern (Gill, 1980), with a Kelvin wave-like wedge penetrating into the TIO region, and off-equatorial maxima over the northwest tropical Atlantic and South America continent indicating the Rossby waves. Tropical convection adjusts tropospheric mean temperature close to a moist-adiabatic profile. An SST increase over a convective region acts to warm the tropospheric column (Xie *et al.*, 2009). Note that, different from the weakening of the NTA SST warming from spring to summer, the tropospheric air warming becomes stronger. In addition, the air keeps warming from spring to summer accompanied by the acceleration of the easterly wind over the TIO and NWP regions, thereby an intensification of the NWPSA via Ekman divergence off the equator (Xie *et al.*, 2009), tightly linked with the increases in the positive NIO SST anomalies (Figure 7e–h). In addition to the WES mechanism for the TIO SST warming related to the easterly anomalies, the troposphere warming can cause an increase in the tropospheric water vapour content, enhancing the moist static energy. The correlation coefficients between the 850-hPa specific humidity anomalies and the PC1 of the right heterogeneous field of the SVD analysis for the inter-member anomalies of SST illustrate that the specific humidity increases from spring to

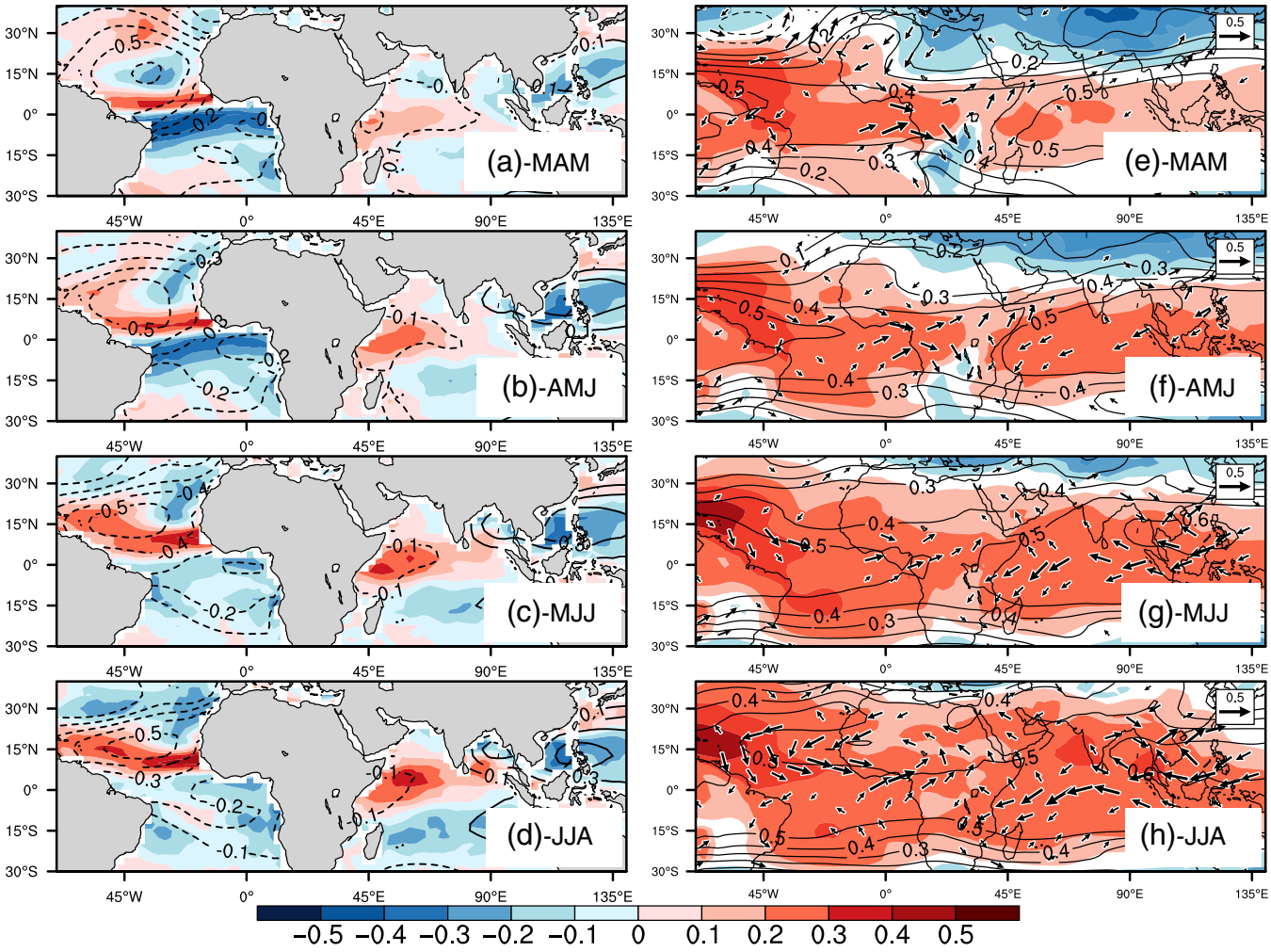

FIGURE 8 Correlation coefficients between the precipitation (a–d; colour shadings), SLP (a–d; contours), tropospheric mean temperature (e–h; colour shadings), 500-hPa geopotential height (e–h; contours) and wind (e–h; vectors) anomalies in (a, e) MAM(1), (b, f) AMJ(1), (c, g) MJJ(1), (d, h) JJA(1) and the PC1 of the right heterogeneous field of the SVD analysis for the inter-member anomalies of SST over the tropical Atlantic, TIO, and NWP regions in the hindcasts. Only the correlations significant at the 95% confidence level are shown [Colour figure can be viewed at wileyonlinelibrary.com]

summer accompanying the SST warming (not shown). The increased atmospheric boundary layer specific humidity induces the reduction of the evaporation, contributing to the SST warming (Chiang and Lintner, 2005).

The correlation coefficients between the 850-hPa velocity potential and divergent wind anomalies and the PC1 of the right heterogeneous field of the SVD analysis for the inter-member anomalies of SST are shown in Figure 9a–d. Centres of low (high) velocity potential are associated with divergent outflow (convergent inflow) winds. Low-level convergences are located over the NTA region from spring to summer, consistent with the precipitation anomalies (Figure 8a–d). Over the western TIO region, low-level winds converge, evolving from spring to summer, resulting in ascending motion, and further increased precipitation, as illustrated in Figure 8a–d. Over the NWP region, low-level divergence enhances from spring to summer, an implication of the NWPSA intensification.

Figure 9e–h shows the regression coefficients between the 200-hPa velocity potential, divergent wind anomalies and the PC1 of the right heterogeneous field of the SVD analysis for the inter-member anomalies of SST. Generally, areas with low-level convergences correspond to those with upper-level divergences, vice versa. Low-level winds converge and upper-level diverge over the NTA region, while divergence and convergence occur at the lower and upper levels over the NWP region, respectively. This indicates that the NTA SST warming forces a local upward motion, leading to a descending branch over the NWP region. This descent gives rise to the low-level easterly wind anomalies, causing the SST warming in the TIO region, mediated by the (WES) feedback (Xie and Philander, 1994), and an intensification of the

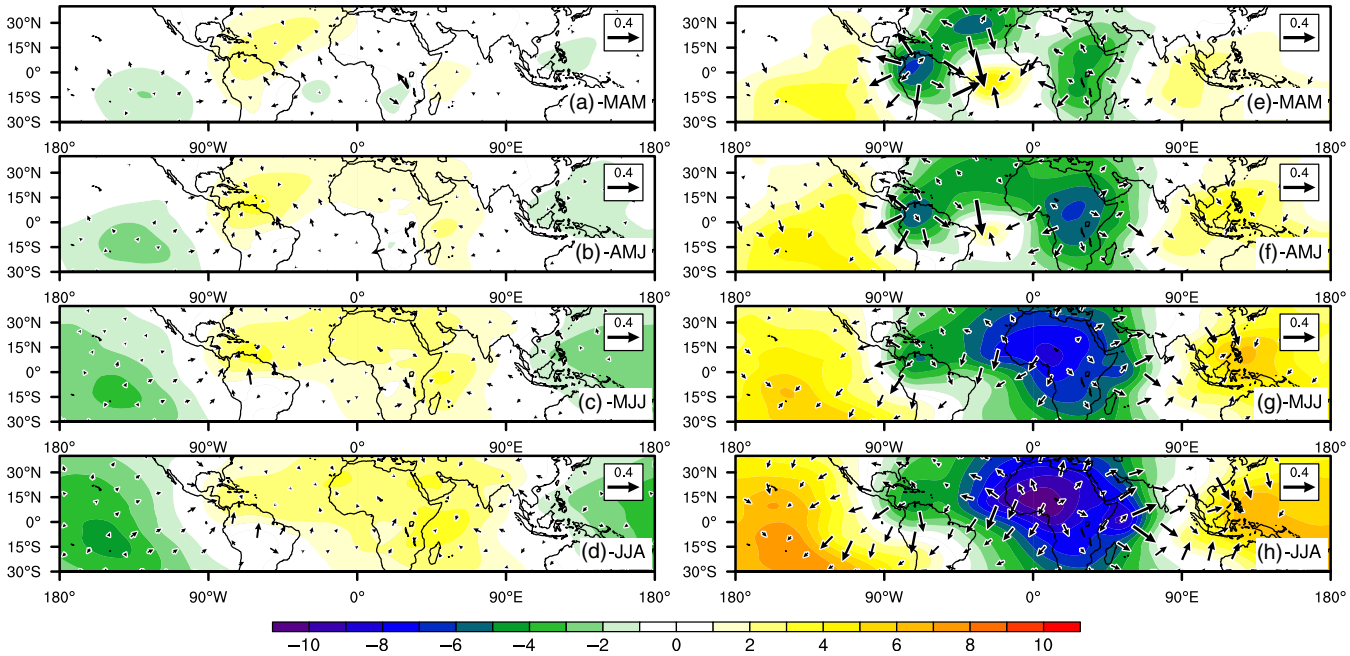

FIGURE 9 Regression coefficients of the 850-hPa velocity potential (colour shadings; units: 10^6 m^2 s^{-1}), divergent wind (vectors; units: m s^{-1}) anomalies in (a) MAM(1), (b) AMJ(1), (c) MJJ(1), (d) JJA(1) onto the PC1 of the right field of the SVD analysis for the inter-member anomalies of SST over the tropical Atlantic, TIO, and NWP regions in the hindcasts. Panels e–h are the same as panels a–d, but for the 200-hPa velocity potential (colour shadings) and divergent wind (vectors) anomalies. Only the correlations significant at the 95% confidence level are shown [Colour figure can be viewed at wileyonlinelibrary.com]

NWPSA via Ekman divergence off the equator (Xie *et al*., 2009).

Finally, we check the regression coefficients between the heat flux, radiation flux (positive downward) anomalies onto the PC1 of the right heterogeneous field of the SVD analysis for the inter-member anomalies of SST. We argue that the low-level wind and SST are coupled, forming a local positive feedback. Figure 10a–d shows that the upward latent heat fluxes are reduced in response to low-level westerly anomalies over the trade wind-prevailing NTA region, contributing to the local SST warming. The positive latent heat fluxes enhance from spring to summer, consistent with the SST variation features (Figure 7e–h). This indicates that the latent heat flux anomalies over the TIO region also act as an important role in the local SST warming. As pointed out above, the increased atmospheric boundary layer specific humidity caused by the troposphere warming can also contribute to the reduction of the latent heat flux, finally giving rise to the SST warming (Chiang and Lintner, 2005).

In addition, the shortwave radiation fluxes increase over the NTA and TIO regions, in favour of the SST warming. Note that the latent heat flux and shortwave radiation flux act as opposite roles in the equatorial Atlantic and southwest TIO regions. The anomaly pattern of the sensible heat flux is generally similar to that of the latent heat flux, but with smaller magnitudes (Figure 10e–h), suggesting that the sensible heat flux makes a minor contribution to the SST warming. In addition, the longwave radiation flux acts to decrease and increase the SST in regions off and near the equatorial Atlantic, respectively. Over the TIO region, positive longwave radiation fluxes move northward from the equatorial region from spring to summer, contributing to the northward migration of the SST warming. However, due to its small magnitude, longwave radiation flux also plays a minor role.

5 | SUMMARY AND DISCUSSION

Using the fifth generation reanalysis of ECMWF, HadISST data, and ENSEMLES hindcasts, this study investigates the impact of the NTA SST anomalies in the ensuing spring of El Niño on the TIO and NWP by applying the methods of composites, SVD, and correlations. The NTA SST warming in the decay spring of El Niño induces a Gill-type response of the overlying atmosphere. The eastward propagating Kelvin wave over the TIO causes the anomalous easterlies in the TIO and NWP regions. The NWPSA is further strengthened via Ekman divergence off the equator. In addition, the NTA SST warming gives rise to a local upward motion, causing a

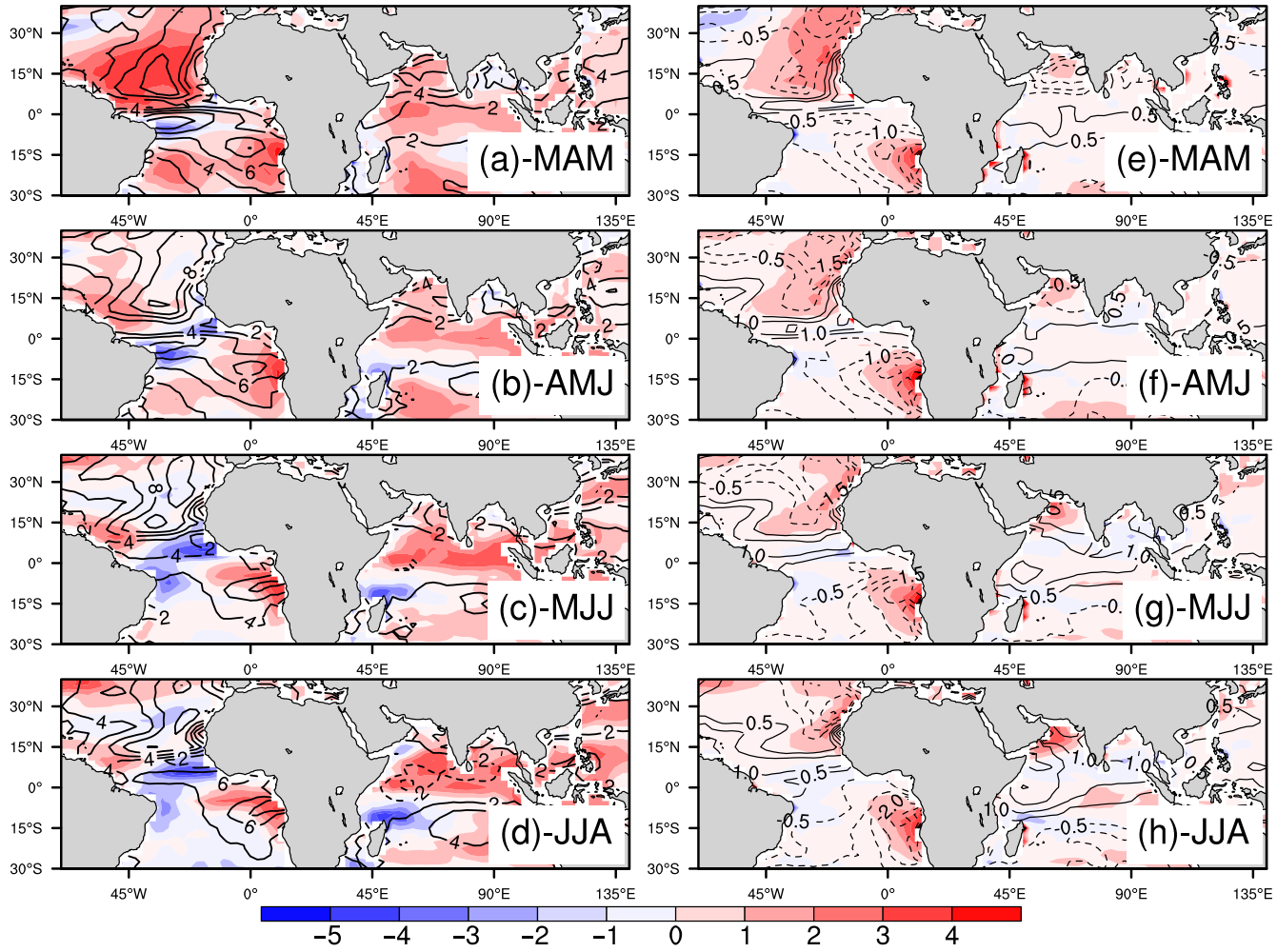

FIGURE 10 Regression coefficients of the latent heat flux (a–d; colour shadings; units: W m^{-2}), net shortwave radiation flux (a–d; contours; units: W m^{-2}), sensible heat flux (e–h; colour shadings; units: W m^{-2}), and net longwave radiation flux (e–h; contours; units: W m^{-2}) anomalies in (a, e) MAM(1), (b, f) AMJ(1), (c, g) MJJ(1), (d, h) JJA(1) onto the PC1 of the right field of the SVD analysis for the inter-member anomalies of SST over the tropical Atlantic, TIO, and NWP regions in the hindcasts [Colour figure can be viewed at wileyonlinelibrary.com]

descent over the NWP region. This descent also contributes to the low-level easterly anomalies and further an intensification of the NWPSA. This study captures both the roles of the eastward propagating Kelvin wave signal (Kucharski *et al*., 2007, 2008, 2009) and the modification of the Walker circulation (Hong *et al*., 2014, 2015; Jin and Huo, 2018) in the impact of the NTA SST anomalies on the TIO and NWP regions.

The anomalous easterlies in the TIO and NWP regions weaken the background southwesterly monsoon, suppressing upward latent heat fluxes. Additionally, the increased atmospheric boundary layer specific humidity caused by the NTA induced-troposphere warming reduces the upward latent heat fluxes. Both these processes contribute to the warming of the TIO region. Additionally, shortwave radiation flux also makes contributions to the SST warming. This study indicates that the second warming of the NIO region in the following summer of El Niño may partially arise from the NTA warming in the ensuing spring of El Niño.

Recently, the contribution of the Atlantic in the pan–tropical ocean–atmosphere interactions is found to be larger than previously thought (Cai *et al*., 2019). The Atlantic SST variability plays a significant role in the SST anomalies over the Indo-Pacific regions. This study improves our understanding of the impact of the NTA SST anomalies in the El Niño decay spring on the TIO and NWP regions, and emphasizes the importance of the NTA region in the pantropical inter-basin interactions.

An important implication of this study is that the NWPSA and NIO SST variability in summer is not only related to the preceding ENSO, but also influenced by the NTA SST anomalies. Hence, correct prediction of ENSO is insufficient to predict the NWPSA and the NIO SST. The NTA SST anomaly also has to be taken into consideration.

ACKNOWLEDGEMENTS

This work is jointly supported by the National Key Research and Development Program of China (2017YFA0604100), the National Natural Science Foundation of China (41805051), and the Startup Foundation for Introducing Talent of NUIST (2017r057).

ORCID

Jing Ma https://orcid.org/0000-0003-3365-656X

REFERENCES

Alexander, M. and Scott, J. (2002) The influence of ENSO on air–sea interaction in the Atlantic. *Geophysical Research Letters*, 29 (14), 46–44. https://doi.org/10.1029/2001GL014347.

Bjerknes, J. (1969) Atmospheric teleconnections from the equatorial Pacific. *Monthly Weather Review*, 97, 163–172.

Cai, W., Wu, L., Lengaigne, M., Li, T., McGregor, S., Kug, J.S., Yu, J. Y., Stuecker, M.F., Santoso, A., Li, X., Ham, Y.G., Chikamoto, Y., Ng, B., McPhaden, M.J., du, Y., Dommenget, D., Jia, F., Kajtar, J. B., Keenlyside, N., Lin, X., Luo, J.J., Martín-Rey, M., Ruprich-Robert, Y., Wang, G., Xie, S.P., Yang, Y., Kang, S.M., Choi, J.Y., Gan, B., Kim, G.I., Kim, C.E., Kim, S., Kim, J.H. and Chang, P. (2019) Pantropical climate interactions. *Science*, 363, eaav4236. https://doi.org/10.1126/science.aav4236.

Chang, P., Fang, Y., Saravanan, R., Ji, L. and Seidel, H. (2006) The cause of the fragile relationship between the Pacific El Niño and the Atlantic El Niño. *Nature*, 443, 324–328. https://doi.org/10.1038/nature05053.

Chen, W., Park, J.-K., Dong, B., Lu, R. and Jung, W.-S. (2012) The relationship between El Niño and the western North Pacific summer climate in a coupled GCM: role of the transition of El Niño decaying phases. *Journal of Geophysical Research: Atmospheres*, 117(D12), 18. https://doi.org/10.1029/2011jd017385.

Chen, W., Lee, J.-Y., Ha, K.-J., Yun, K.-S. and Lu, R. (2016) Intensification of the Western North Pacific anticyclone response to the short decaying El Niño event due to greenhouse warming. *J Clim*. Published online. http://dx.doi.org/10.1175/JCLI-D-15-0195.1

Chen, W., Lee, J.-Y., Lu, R., Dong, B. and Ha, K.-J. (2014a) Intensified impact of tropical Atlantic SST on the western North Pacific summer climate under a weakened Atlantic thermohaline circulation. *Climate Dynamics*, 45, 1–14. https://doi.org/10.1007/s00382-014-2454-4.

Chen, W., Lu, R. and Dong, B. (2014b) Intensified anticyclonic anomaly over the western North Pacific during El Niño decaying summer under a weakened Atlantic thermohaline circulation. *Journal of Geophysical Research–Atmosphere*, 119, 13637–13650. https://doi.org/10.1002/2014JD022199.

Chen, S., Wu, R. and Chen, W. (2015) The changing relationship between interannual variations of the North Atlantic Oscillation and northern tropical Atlantic SST. *Journal of Climate*, 28, 485–504. https://doi.org/10.1175/JCLI–D–14–00422.1.

Chiang, J. and Lintner, B. (2005) Mechanisms of remote tropical surface warming during El Niño. *Journal of Climate*, 18(20), 4130–4149.

Chiang, J. and Sobel, A. (2002) Tropical tropospheric temperature variations caused by ENSO and their influence on the remote tropical climate. *Journal of Climate*, 15(18), 2616–2631.

Chowdary, J.S., Harsha, H.S., Gnanaseelan, C., Srinivas, G., Parekh, A., Pillai, P. and Naidu, C.V. (2017) Indian summer monsoon rainfall variability in response to differences in the decay phase of El Niño. *Climate Dynamics*, 48(7), 2707–2727. https://doi.org/10.1007/s00382-016-3233-1.

Chowdary, J.S., Patekar, D., Srinivas, G., Gnanaseelan, C. and Parekh, A. (2019) Impact of the Indo-Western Pacific Ocean Capacitor mode on South Asian summer monsoon rainfall. *Climate Dynamics*, 53(3), 2327–2338. https://doi.org/10.1007/s00382-019-04850-w.

Copernicus Climate Change Service (C3S) (2017). ERA5: Fifth generation of ECMWF atmospheric reanalyses of the global climate. Copernicus Climate Change Service Climate Data Store (CDS), 12/01/2018. https://cds.climate.copernicus.eu/cdsapp#!/dataset/reanalysis–era5–pressure–levels–monthly–means?tab=form.

Deser, C. and Timlin, M.S. (1997) Atmosphere–ocean interaction on weekly timescales in the North Atlantic and Pacific. *Journal of Climate*, 10, 393–408.

Deser, C., Alexander, M.A., Xie, S.–.P., et al. (2010) Sea surface temperature variability: patterns and mechanisms. *Annual Review of Marine Science*, 2, 115–143.

Du, Y., Xie, S.–.P., Huang, G., et al. (2009) Role of air–sea interaction in the long persistence of El Niño–induced north Indian Ocean warming. *Journal of Climate*, 22(8), 2023–2038.

Enfield, D. and Mayer, D. (1997) Tropical Atlantic SST variability and its relation to El Niño–Southern Oscillation. *Journal of Geophysical Research: Oceans*, 102, 929–945. https://doi.org/10.1029/96jc03296.

García–Serrano, J., Cassou, C., Douville, H., et al. (2017) Revisiting the ENSO teleconnection to the tropical North Atlantic. *Journal of Climate*, 30(17), 6945–6957.

Giannini, A., Kushnir, Y. and Cane, M.A. (2000) Interannual variability of Caribbean rainfall, ENSO, and the Atlantic Ocean. *Journal of Climate*, 13(2), 297–311.

Giannini, A., Chiang, J., Cane, M., Kushnir, Y. and Seager, R. (2001) The ENSO Teleconnection to the Tropical Atlantic Ocean: Contributions of the Remote and Local SSTs to Rainfall Variability in the Tropical Americas. *Journal of Climate*, 14, 4530–4544. https://doi.org/10.1175/1520–0442(2001)014<4530:tetttt>2.0.co;2.

Gill, A.E. (1980) Some simple solutions for heat–induced tropical circulation. *Quarterly Journal of the Royal Meteorological Society*, 106(449), 447–462.

Ham, Y.–.G., Kug, J.–.S., Park, J.–.Y. and Jin, F.–.F. (2013) Sea surface temperature in the north tropical Atlantic as a trigger for El Niño/Southern Oscillation events. *Nature Geoscience*, 6, 112–116. https://doi.org/10.1038/ngeo1686.

Hong, C.–.C., Chang, T.–.C. and Hsu, H.–.H. (2014) Enhanced relationship between the tropical Atlantic SST and the summertime western North Pacific subtropical high after the early 1980s. *Journal of Geophysical Research–Atmosphere*, 119, 3715–3722.

Hong, C.–.C., Lee, M.–.Y., Hsu, H.–.H., Lin, N.–.H. and Tsuang, B.–J. (2015) Tropical SST forcing on the anomalous WNP subtropical high during July–August 2010 and the record–high SST in the tropical Atlantic. *Climate Dynamics*, 45, 633–650. https://doi.org/10.1007/s00382–014–2275–5.

Jiang, W., Huang, G., Huang, P. and Hu, K. (2018) Weakening of northwest Pacific anticyclone anomalies during post–El Niño summers under global warming. *Journal of Climate*, 31(9), 3539–3555. https://doi.org/10.1175/jcli-d-17-0613.1.

Jin, D. and Huo, L. (2018) Influence of tropical Atlantic sea surface temperature anomalies on the East Asian summer monsoon. *Quarterly Journal of the Royal Meteorological Society*, 144(714), 1490–1500. https://doi.org/10.1002/qj.3296.

Kamae, Y., Li, X., Xie, S.-P. and Ueda, H. (2017) Atlantic effects on recent decadal trends in global monsoon. *Climate Dynamics*, 49 (9), 3443–3455. https://doi.org/10.1007/s00382-017-3522-3.

Klein, S.A., Soden, B.J. and Lau, N.C. (1999) Remote sea surface temperature variations during ENSO: evidence for a tropical atmospheric bridge. *Journal of Climate*, 12(4), 917–932.

Kucharski, F., Bracco, A., Yoo, J.H. and Molteni, F. (2007) Low–frequency variability of the Indian monsoon–ENSO relationship and the tropical Atlantic: the "weakening" of the 1980s and 1990s. *Journal of Climate*, 20(16), 4255–4266. https://doi.org/10.1175/jcli4254.1.

Kucharski, F., Bracco, A., Yoo, J.H. and Molteni, F. (2008) Atlantic forced component of the Indian monsoon interannual variability. *Geophysical Research Letters*, 35, L04706. https://doi.org/10.1029/2007GL033037.

Kucharski, F., Bracco, A., Yoo, J.H., Tompkins, A.M., Feudale, L., Ruti, P. and Dell'Aquila, A. (2009) A Gill–Matsuno–type mechanism explains the tropical Atlantic influence on African and Indian monsoon rainfall. *Quarterly Journal of the Royal Meteorological Society*, 135(640), 569–579. https://doi.org/10.1002/qj.406.

Lee, S.K., Enfield, D.B. and Wang, C. (2008) Why do some El Niños have no impact on tropical North Atlantic SST? *Geophysical Research Letters*, 35(16), 5. https://doi.org/10.1029/2008GL034734.

Li, C.F., Lu, R.Y. and Dong, B.W. (2014) Predictability of the western North Pacific summer climate associated with different ENSO phases by ENSEMBLES multi–model seasonal forecasts. *Climate Dynamics*, 43(7–8), 1829–1845. https://doi.org/10.1007/s00382–013–2010–7.

Li, X.C., Xie, S.P., Gille, S.T. and Yoo, C. (2016) Atlantic-induced pan-tropical climate change over the past three decades. *Nature Climate Change*, 6(3), 275–280. https://doi.org/10.1038/NCLIMATE2840.

Li, T., Wang, B., Wu, B., Zhou, T., Chang, C.-P. and Zhang, R. (2017) Theories on formation of an anomalous anticyclone in western North Pacific during El Niño: a review. *Journal of Meteorological Research*, 31(6), 987–1006. https://doi.org/10.1007/s13351-017-7147-6.

Lin, H., Derome, J. and Brunet, G. (2007) The nonlinear transient atmospheric response to tropical forcing. *Journal of Climate*, 20 (22), 5642–5665. https://doi.org/10.1175/2007jcli1383.1.

van der Linden, P. and Mitchell, J.F.B. (Eds.). (2009) *ENSEMBLES: Climate Change and its Impact: Summary of Research and Results from ENSEMBLES Project*. Exeter: Met Office Hadley Centre, p. 160.

Lintner, B. and Chiang, J. (2007) Adjustment of the remote tropical climate to El Niño conditions. *Journal of Climate*, 20, 2544–2557. https://doi.org/10.1175/jcli4138.1.

Ma, J., Xie, S.–.P. and Xu, H. (2017a) Inter–member variability of the summer Northwest Pacific subtropical anticyclone in the ensemble forecast. *Journal of Climate*, 30, 3927–3941. https://doi.org/10.1175/JCLI–D–16–0638.1.

Ma, J., Xie, S.–.P. and Xu, H. (2017b) Contributions of the North Pacific meridional mode to ensemble spread of ENSO prediction. *Journal of Climate*, 30(22), 9167–9181.

Rayner, N.A., Parker, D.E., Horton, E.B., et al. (2003) Global analyses of sea surface temperature, sea ice, and night marine. *Journal of Geophysical Research–Atmosphere*, 108, D14. https://doi.org/10.1029/2002JD002670.

Rong, X.Y., Zhang, R.H. and Li, T. (2010) Impacts of Atlantic sea surface temperature anomalies on Indo–East Asian summer monsoon–ENSO relationship. *Chinese Science Bulletin*, 55, 2458–2468.

Trenberth, K.E., Branstator, G., Karoly, D., et al. (1998) Progress during TOGA in understanding and modeling global teleconnections associated with tropical sea surface temperatures. *Journal of Geophysical Research–Atmosphere*, 103, 14291–14324. https://doi.org/10.1029/97JC01444.

Wang, C. (2004) ENSO, Atlantic Climate Variability, and the Walker and Hadley Circulations. Diaz, H.F. and Bradley, R.S. (eds.) *The Hadley Circulation: Present, Past and Future*. Netherlands: Kluwer Academic Publishers, pp. 173–202. https://doi.org/10.1007/978–1–4020–2944–8_6.

Wang, B., Wu, R.G. and Fu, X.H. (2000) Pacific-East Asian teleconnection: how does ENSO affect East Asian climate? *Journal of Climate*, 13(9), 1517–1536. https://doi.org/10.1175/1520-0442(2000)013<1517:Peathd>2.0.Co;2.

Xie, S.P. and Philander, S.G.H. (1994) A coupled ocean–atmosphere model of relevance to the ITCZ in the eastern Pacific. *Tellus A*, 46(4), 340–350. https://doi.org/10.1034/J.1600–0870.1994.T01–1–00001.X.

Xie, S.–.P., Hu, K., Hafner, J., et al. (2009) Indian Ocean capacitor effect on indo–western Pacific climate during the summer following El Niño. *Journal of Climate*, 22(3), 730–747. https://doi.org/10.1175/2008jcli2544.1.

Xie, S.-P., Du, Y., Huang, G., Zheng, X.-T., Tokinaga, H., Hu, K. and Liu, Q. (2010) Decadal shift in El Niño influences on indo–western Pacific and east Asian climate in the 1970s. *Journal of Climate*, 23(12), 3352–3368. https://doi.org/10.1175/2010jcli3429.1.

Xie, S.–.P., Kosaka, Y., Du, Y., et al. (2016) Indo–western Pacific Ocean capacitor and coherent climate anomalies in post–ENSO summer: a review. *Advances in Atmospheric Sciences*, 33(4), 411–432. https://doi.org/10.1007/s00376–015–5192–6.

Yang, J.L., Liu, Q.Y., Xie, S.-P., et al. (2007) Impact of the Indian Ocean SST basin mode on the Asian summer monsoon. *Geophysical Research Letters*, 34, L02708. https://doi.org/10.1029/2006GL028571.

Zhou, Z.-Q., Zhang, R. and Xie, S.-P. (2019) Interannual variability of summer surface air temperature over Central India: implications for monsoon onset. *Journal of Climate*, 32, 1693–1706. https://doi.org/10.1175/jcli-d-18-0675.1.

How to cite this article: Ma J, He W, Chen Z, Fu Y, Yin J. The impact of north tropical Atlantic sea surface temperature anomalies in the ensuing spring of El Niño on the tropical Indian Ocean and Northwest Pacific. *Int J Climatol*. 2020;1–14. https://doi.org/10.1002/joc.6500